Astron. Astrophys. 342, 531–541 (1999)

ASTRONOMY AND ASTROPHYSICS

Dynamic model atmospheres of AGB stars

II. Synthetic near infrared spectra of carbon stars

R. Loidl[1], **S. Höfner**[2], **U.G. Jørgensen**[2], **and B. Aringer**[1]

[1] Institut für Astronomie der Universität Wien, Türkenschanzstrasse 17, A-1180 Wien, Austria
[2] Niels Bohr Institute, Astronomical Observatory, Juliane Maries Vej 30, DK-2100 Copenhagen, Denmark

Received 25 August 1998 / Accepted 17 November 1998

Abstract. We have calculated synthetic opacity sampling spectra for carbon-rich Asymptotic Giant Branch (AGB) stars based on dynamic model atmospheres presented in the first paper of this series. We discuss how different model parameters influence the resulting synthetic spectra and how the spectra vary with phase. The molecules included are: CO, CH, CN, C_2, HCN, C_2H_2 and C_3. We show in which atmospheric layers the different molecules form, in an attempt to understand the qualitatively different variation with pulsation phase exhibited by various spectral features. Almost all features are blends of transitions from more than one molecule, and we therefore identify the most important transitions and molecules that contribute to the main spectral features from 0.5 to 12 μm. Furthermore, we demonstrate the effect on the individual spectral features due to the carbon depletion when dust is formed in the atmosphere.

Key words: stars: carbon – stars: atmospheres – stars: AGB and post-AGB – stars: variables: general – radiative transfer – hydrodynamics

1. Introduction

Large amplitude pulsations with periods of about 100 to 1000 days are characteristic for stars on the Asymptotic Giant Branch (AGB). In their atmospheres, the density-temperature structure is highly dependent on dynamical phenomena, such as shock waves and stellar winds. In addition, the formation of molecules and dust grains plays a very important role. Stellar pulsation creates strong shock waves in the atmosphere which cause a levitation of the outer layers. The dust-free inner parts of the atmosphere are modulated by the propagating shock waves which affect the observable properties and cannot be simulated using hydrostatic model atmospheres (Aringer et al. 1999, Alvarez & Plez 1998, Höfner et al. 1998a).

In the past, observed spectra of cool stars have been mostly analysed with synthetic spectra calculated from hydrostatic model atmospheres (e.g. Jørgensen 1989a, Lambert et al. 1986, Goebel et al. 1980 for carbon-rich stars; Tsuji et al. 1997 for oxygen-rich stars) or with simple blackbodies (e.g. Goebel et al. 1980). Spectra based on hydrostatic models are appropriate for the description of giants showing no significant pulsation. But for an investigation of the effects of various time-dependent phenomena (shocks, stellar winds) on observable properties of pulsating AGB stars the use of dynamic models is the only self-consistent method.

Due to new instrumental developments during the last few years more and better observational data on AGB stars became available. The very successful ISO mission provides for the first time full spectral coverage of the wavelength range between 2.5 and 197.6 μm and multi-epoch spectroscopic observations of carbon-rich AGB variables. This has made the shortcomings of hydrostatic standard model atmospheres more apparent, especially with regard to temporal variations in observed spectra and in photometric colours which are connected to stellar pulsation.

In the last few years, considerable progress has been made with regard to modelling of AGB star atmospheres. Bessell et al. (1989, 1996) have computed the first synthetic spectra for oxygen rich AGB stars based on dynamic model atmospheres, and Beach et al. (1988) analysed effects of pulsation on apparent diameters and broad band fluxes. For carbon-rich objects, Fleischer et al. (1992) and Höfner & Dorfi (1997) have presented the first dynamic models which include dust formation in a self-consistent way. For these models of circumstellar envelopes qualitative agreement with observable quantities like IR light curves (Winters et al. 1997) or IRAS colours (Windsteig et al. 1997) could be obtained.

So far, dynamical modelling of C-stars has mainly concentrated on objects with high mass loss rates and more or less optically thick dust envelopes, investigating the properties of the circumstellar dust shells and mass loss by dust-driven stellar winds. In paper I of this series (Höfner et al. 1998b; HJLA98 from now on) on dynamical model atmospheres of AGB stars we focused on the structure of the inner dust-free atmospheric regions. The visual and near infrared absorption spectra are mainly formed there in AGB stars which are not completely obscured by an optically thick dust envelope. An improvement of the dynamical models by introducing a more realistic treatment of the gas opacity than in earlier C-rich models was necessary in order to obtain reasonable atmospheric structures and realistic molecular features.

Send offprint requests to: R. Loidl (loidl@astro.univie.ac.at)

Table 1. Model parameters ($L_\star$, $M_\star$, $T_\star$, $\varepsilon_{\rm C}/\varepsilon_{\rm O}$, P, $\Delta u_{\rm p}$) and results: luminosity variation $\Delta m_{\rm bol}$, mass loss rate $\dot{M}$, mean degree of condensation at the outer boundary $f_{\rm cond}$ and the corresponding dust-to-gas ratio $\rho_{\rm d}/\rho_{\rm g}$. For convenience we also list $R_\star$ and lg $g_\star$ (calculated from the other stellar parameters). A ″-″ means that the model does not show mass loss by a stellar wind, a ″T″ indicates a transition model between a dust free dynamic atmosphere and a dust-driven stellar wind (some dust is present but no outflow occurs).

model	$L_\star$ $[L_\odot]$	$M_\star$ $[M_\odot]$	$T_\star$ [K]	$R_\star$ $[R_\odot]$	lg $g_\star$	$\varepsilon_{\rm C}/\varepsilon_{\rm O}$	P [d]	$\Delta u_{\rm p}$ [km s^{-1}]	$\Delta m_{\rm bol}$	$\dot{M}$ $[M_\odot/yr]$	$f_{\rm cond}$	$\rho_{\rm d}/\rho_{\rm g}$ $[10^{-3}]$
P5C14U2	5000	1.0	2970	267	−0.42	1.40	295	2.0	0.22	–	–	–
P7C12U4	7000	1.0	2880	336	−0.61	1.20	390	4.0	0.44	–	–	–
P7C14U2	7000	1.0	2880	336	−0.61	1.40	390	2.0	0.22	–	–	–
P7C14U4	7000	1.0	2880	336	−0.61	1.40	390	4.0	0.44	T	(0.3)	(0.7)
P7C18U4	7000	1.0	2880	336	−0.61	1.80	390	4.0	0.44	$2.2 \cdot 10^{-7}$	0.13	0.6
P10C14U4	10000	1.0	2790	428	−0.82	1.40	525	4.0	0.44	$6.6 \cdot 10^{-7}$	0.19	0.4
P10C18U2	10000	1.0	2790	428	−0.82	1.80	525	2.0	0.22	$1.9 \cdot 10^{-7}$	0.05	0.2
P10C18U4	10000	1.0	2790	428	−0.82	1.80	525	4.0	0.44	$1.0 \cdot 10^{-6}$	0.14	0.6
P13C12U4	13000	1.0	2700	521	−0.99	1.20	650	4.0	0.44	$5.7 \cdot 10^{-7}$	0.33	0.4
P13C14U4	13000	1.0	2700	521	−0.99	1.40	650	4.0	0.44	$2.9 \cdot 10^{-6}$	0.25	0.6
P7MC14U2	7000	1.4	2880	336	−0.47	1.40	390	2.0	0.22	–	–	–
P7MC14U4	7000	1.4	2880	336	−0.47	1.40	390	4.0	0.44	–	–	–
P10MC14U4	10000	1.4	2790	428	−0.67	1.40	525	4.0	0.44	T	(0.3)	(0.7)
P7TC14U4	7000	1.0	2970	316	−0.56	1.40	390	4.0	0.44	–	–	–
P10TC14U4	10000	1.0	2880	401	−0.77	1.40	525	4.0	0.44	$5.7 \cdot 10^{-7}$	0.19	0.4

In this paper we present a systematic discussion of the synthetic opacity sampling spectra resulting from these improved hydrodynamic models. A comparison of selected model spectra with ISO observations can be found in Hron et al. (1998). Aringer et al. (1999) recently presented a paper showing that our dynamical models are in principle able to explain the whole range of equivalent widths of observed SiO bandheads in oxygen-rich AGB stars and their variations.

2. Hydrodynamic models and spectral synthesis

2.1. Dynamic models

We use the dynamic model atmospheres of HJLA98 for the calculation of synthetic spectra. To obtain the atmospheric structure, the coupled system of grey radiation hydrodynamics and time-dependent dust formation is solved. The dust formation is treated by the so-called moment method (Gail & Sedlmayr 1988, Gauger et al. 1990). A set of four equations which describe the time-dependent formation, growth and evaporation of grains is solved simultaneously with the radiation-hydrodynamics, providing information about the number density and average size of the grains, and the fraction of condensible material actually condensed into dust particles (degree of condensation). These quantities are sufficient to derive e.g. the dust opacity (provided the dust grains are small compared to the relevant wavelengths which is a fair approximation in this context) and to describe the effects of the newly formed grains on the dynamical atmosphere. Details about the modelling method can be found in HJLA98 and references therein.

The dynamical calculations start with a hydrostatic initial model which represents the hydrostatic limit case of the grey radiation hydrodynamics equations. It can be directly compared to standard model atmospheres (see HJLA98). The stellar pulsation of the AGB star is simulated by a variable boundary (piston) located beneath the stellar photosphere as introduced by Bowen (1988). The piston varies sinusoidally with a velocity amplitude $\Delta u_{\rm p}$ and a period P.

A relatively severe limitation that is imposed on state–of–the–art dynamic model atmospheres by computing time requirements is the restriction to grey radiative transfer. The hydrostatic limit case provides an opportunity to test the effects of grey radiative transfer by comparing the atmospheric structures to classical model atmospheres which include a detailed frequency-dependent treatment of the radiative transfer. As demonstrated in HJLA98 the use of reasonable mean opacities (e.g. Planck means based on molecular data) leads to a structure of the atmosphere that is in relatively good agreement with a frequency-dependent model based on the same opacity input data.

The models are characterized by the following set of parameters: stellar mass $M_\star$, luminosity $L_\star$, effective temperature $T_\star$ of the hydrostatic initial model and the carbon-to-oxygen abundance ratio $\varepsilon_{\rm C}/\varepsilon_{\rm O}$ as well as the piston period P and velocity amplitude $\Delta u_{\rm p}$. All abundances except that of carbon are assumed to be solar. $T_\star$ has been calculated from $M_\star$ and $L_\star$ using the radius–luminosity–mass relation of Iben (1984) with $(l/H_p) = 0.90$ and $Z = 0.020$ as in Bowen & Willson (1991). P was chosen according to a period–luminosity relation for Miras (Feast et al. 1989).

The models used for the calculation of the synthetic spectra are summarized in Table 1. In contrast to many earlier dynamic models of carbon stars in the literature which simply use a constant gas absorption coefficient independent of the thermody-

namical conditions, these models are based on opacities derived from detailed molecular data (Jørgensen 1997). This has a dramatic influence on the atmospheric structure and the resulting mass loss rates (see HJLA98) as well as on the synthetic spectra (Höfner et al. 1998a; see also below).

2.2. Spectral synthesis

The dynamical calculation yields the structure of the atmosphere and circumstellar envelope (density, temperature, degree of condensation, etc.) as a function of time. The hydrodynamic models are calculated using a grey radiative transfer and they are all optically thick at the inner boundary. However, when using a detailed frequency-dependent radiative transfer for the computation of the synthetic spectra, it might happen that at some frequencies they are not optically thick. To avoid this problem, we extended the models inwards by solving the stellar structure equations. The effect of dynamical phenomena on the spectra are not important in those parts of the atmosphere which are concerned by this extension, therefore the hydrostatic equations are appropriate for the description.

Based on this structure we computed the synthetic spectra by evaluating (1) the chemical abundances using an equilibrium chemistry, (2) the continuum absorption using routines from the MARCS code (Gustafsson et al. 1975 in the version of Jørgensen et al. 1992) and (3) the molecular opacities as a function of wavelength using the opacity sampling method. The chemistry routines are those of Tsuji (1973), with updated data as described in Helling et al. (1996) except for data for C_3 which are from Irwin (1981).

In the spectral synthesis code, opacity sampling tables are read, the total opacity and the source function in each layer are calculated and the detailed transfer equation in plane parallel geometry solved. The depletion of carbon in the gas phase by dust formation is taken into account. Opacity data for C_2 are from the work of Querci et al. (1974), data for CO are from Goorvitch & Chackerian (1994), data for CN from the work of Jørgensen & Larsson (1990), data for HCN from Jørgensen et al. (1985), data for C_2H_2 from Jørgensen (recently modified version of unpublished thesis work from 1982), and data for C_3 were taken from Jørgensen et al. (1989b). The molecular opacities were treated in the opacity sampling (OS) approximation (see e.g. Ekberg et al. 1986), and included about 5000 points throughout the spectrum, equally spaced in wavenumber inside 6 intervals (see Jørgensen et al. 1992).

Dynamic models calculated with a constant value for the gas opacity ($\kappa_g = 2 \cdot 10^{-4}$ cm^2/g) as proposed by Bowen (1988; for O-rich Mira models)[1] have lead to inspiring improvements in the understanding of the mass loss process in AGB stars, but have failed to predict a reasonably looking infrared spectrum (Bessell et al. 1989, Loidl et al. 1997). This constant gas absorption coefficient leads to models with artificially high gas pressure for a given temperature. When the structure of such a model is used to compute a synthetic spectrum, it turns out that the computed partial pressures (and hence the total gas opacity) are overestimated to such a degree that the resulting molecular features are almost completely saturated throughout the near-infrared region. In contrast, the present models which are computed with opacities derived from detailed molecular data are able to predict spectra which are in good qualitative agreement with ISO-SWS observations (Hron et al. 1998) and results from hydrostatic models. In the hydrostatic models the radiative transfer is treated in more detail than what is at present possible in the hydrodynamic models, but effects as dust formation and shocks cannot be included.

[1] This constant value was chosen by Bowen (1988) on the basis that it leads to the same structure in the surface layers of a given model of an oxygen-rich Mira star as was obtained with a detailedly calculated Rosseland mean for the same model.

Table 2. Main features in the wavelength range between 0.5 and 10 μm and the contributing molecules:

wavelength [μm]	contributing molecules
0.5 −2	C_2, CN and CH
2.5	C_2H_2, C_2, CO and HCN
3.0	C_2H_2 and HCN
3.8	C_2H_2
4.5 −6	C_3, CO, C_2H_2 and C_2
7 −9	C_3, C_2H_2 and HCN

3. Synthetic spectra

We have computed synthetic opacity sampling spectra including the molecules CO, CH, C_2, CN, HCN, C_2H_2 and C_3 in the wavelength range between 0.5 and 12 μm with a resolution of 800. The spectra have then been rebinned to about a resolution of 100. This is necessary, because opacity sampling is a statistical method. The main features in our spectra are summarized in Table 2. Fig. 1 gives more detailed identifications of the important transitions which are included in our calculations. A common feature of all models is that there are barely continuum points in the NIR region.

3.1. Formation of molecular features

Weak lines in the visual produced by diatomic molecules and the continuum absorption from H^- are examples of spectral features formed in the hot (T higher than approximately 4000 K), dense inner regions of the atmosphere. The upper layers (T lower than approximately 3000 K) are severely affected by hydrodynamical effects. The strong lines of CO and basically all the polyatomic molecular bands observable in the near infrared region are formed in these layers.

Inwards through the stellar atmosphere temperature (T) and gas pressure (P_g) increase. A lower gas pressure generally favours smaller molecules and lower temperatures favour larger molecules. The change of the ratios between the different molecular species through the atmosphere therefore depends

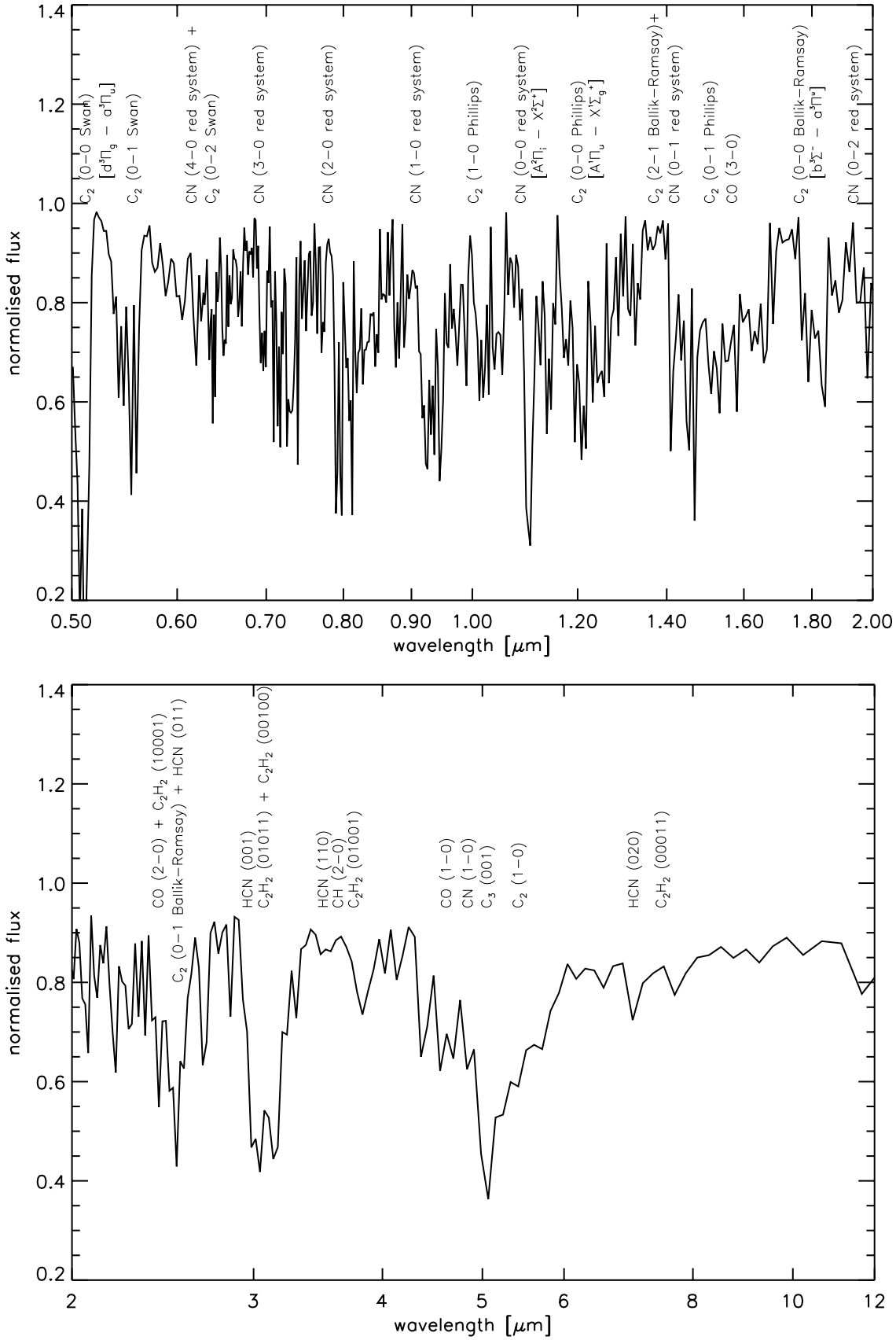

Fig. 1. Identification of the features in the wavelength range between 0.5 and 12 μm.

sensitively on the slope of the T-P_g curve. If the temperature increases rapidly with increasing gas pressure, as it is the case in all known hydrostatic cool atmospheres, the ratio between polyatomic and diatomic molecules will decrease. In connection with shocks in hydrodynamic models, the gas pressure locally increases considerably while the temperature may stay almost constant (depending on the efficiency of radiative cooling). In such regions of the atmosphere the relative importance of polyatomic molecules may again increase inwards. This results in a spatial distribution of the molecules which is much more complex than in a hydrostatic model.

To illustrate these effects with a particular example, we show in Fig. 2 the T-P_g structure of the minimum and maximum light models of P7C14U4 (full $\sim$ phase 1.0 = maximum light, dash-triple-dot $\sim$ phase 0.50 = minimum light). In addition the partial pressures of CO, CN, C_2 (upper panel) and HCN, C_3 and C_2H_2 (middle panel) for the maximum light model are plotted. Note that the location of the propagating shocks changes with phase.

Induced by the shock waves, the gas pressure increases two orders of magnitude around 1600 K in the maximum light model of P7C14U4. As a consequence, the ratio of the polyatomics to diatomics increases, but the effect is not very pronounced because this region is dominated by C_2H_2, anyhow. Behind the shock the ratio decreases again. The next shock occurs between 2000 and 2100 K, there the ratio of the polyatomics to diatomics increases considerably. Due to the shocks the partial pressures of polyatomic molecules have two distinct peaks in the atmosphere. From 2100 to 6000 K the partial pressures of C_2H_2 and C_3 decrease much more rapidly than that of e.g. C_2 due to the increasing temperature and moderately increasing gas pressure.

C_2 forms deep in the atmosphere (see Fig. 2) and its partial pressure increases rapidly at temperatures around and above 2000 K. The bulk of the C_2 band system is in the visual spectral region, but a few relatively strong transitions appear around 2.5 μm arising from regions with T$\gtrsim$2500 K.

The formation of C_3 requires a combination of relatively high partial pressure (in order for the collision probability to be high enough) and low temperature (in order not to dissociate), and its partial pressure therefore has a rather narrow peak around 2000 K. Its main spectral feature is the fundamental C-C stretching at 5 μm which forms around 2000 K.

The formation of C_2H_2 in a hydrogen dominated atmosphere depends less on the density than the one of C_3 because only two non-hydrogen atoms participate in the formation. On the other hand it is much more sensitive to temperature (being four-atomic). As a result, C_2H_2 has a very broad distribution stretching toward much lower temperatures than C_3. This is the reason why C_2H_2 is more important in the grain formation process than C_3. The main spectral features in our C_2H_2 computations are at 3 μm (the well studied fundamental C-H stretching), at 3.8 μm (a relatively strong combination band, not contaminated with other molecular bands), a combination band at 4.7 μm and a broad depression concentrated in the 7 to 8 μm region. An additional C_2H_2 band at 2.5 μm is relatively strong in our computations. All these features originate from layers cooler than 2100 K.

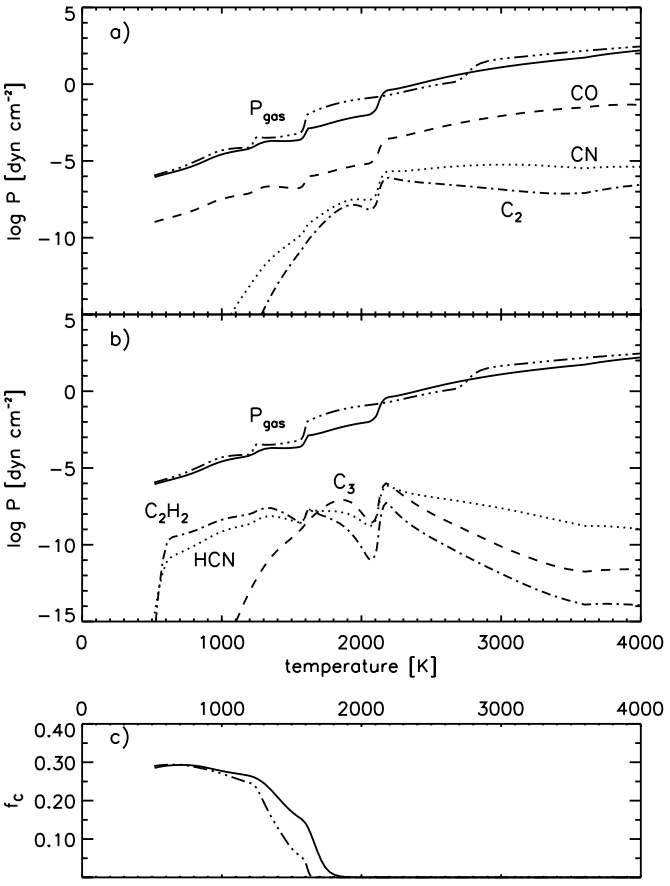

Fig. 2a–c. Gas pressure versus gas temperature for two phases of model P7C14U4 (*upper* and *middle* panel). Full drawn line corresponds to phase 1.00 (maximum light) and dash-triple-dot line to phase 0.50 (minimum light). Dashed, dotted and dash-dotted lines show the partial pressures at maximum light of the diatomics CO, CN and C_2 in **a** and of the polyatomics C_3, HCN and C_2H_2 in **b**. Note the structure of two distinct maxima in the partial pressure for C_2H_2 and the other polyatomics near 2100 and 1600 K in connection with the shocks. In the lower panel the degree of condensation is plotted for the illustration of dust formation for maximum (full) and minimum (dash-triple-dot) light (see text).

HCN is more abundant than C_2H_2 and C_3 in the deeper layers of the atmosphere because it is three-atomic and consists of only 2 non-hydrogen atoms, but its abundance resembles closely that of C_2H_2 in the upper layers, although with approximately an order of magnitude lower partial pressures than C_2H_2 for stars of effective temperatures and C/O ratios discussed here. The strongest HCN band is the C-H fundamental stretching mode at 3 μm. HCN also contributes to absorption in the 7 μm region. The HCN absorption originates from temperatures between 1800 and 3000 K.

The strongest CO band, the fundamental vibration at 5 μm, is strongly blended with the C_2H_2 and C_3 bands in the same region. Its contribution is, however, clearly seen as a broadening of the 5 μm feature, in particular at the short wavelength side of the feature. Also at 2.5 μm the trace of CO (first overtone) is clearly seen, but it is blended with several C_2 bands and a C_2H_2

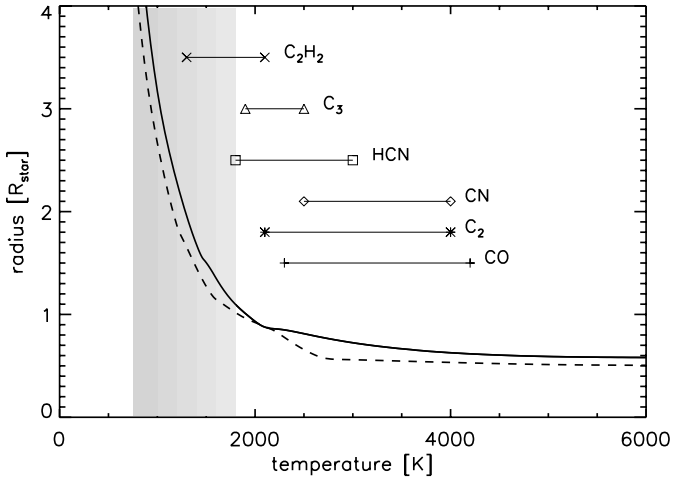

Fig. 3. Radius versus temperature for two phases of model P7C14U4. Full drawn line corresponds to phase 1.00 and dashed line to phase 0.50. The vertical bars indicate the temperature ranges for the molecules CO, C_2, CN, HCN, C_3 and C_2H_2 in which their features between 0.5 and 12 μm are approximately formed. The grey shaded area denotes the region of dust formation.

combination band. The CO features form in regions hotter than about 2300 K.

In Fig. 3 we have plotted radius versus temperature for maximum and minimum light of model P7C14U4. The vertical bars indicate the temperature ranges where the CO, C_2, CN, HCN, C_3 and C_2H_2 features approximately form according to our models. These temperatures of formation were determined by cutting the models (see Table 1) at different temperatures and calculating synthetic spectra for each single molecule. The lower temperature given denotes that where all features (between 0.5 and 12 μm) of the concerned molecule were complete as in the full model and the higher temperature denotes that when all features had completely disappeared. When projecting these temperature ranges onto the curves, one can derive corresponding radii. Table 3 summarizes these results. Dust formation typically starts at around 2 to 3 stellar radii (see Höfner & Dorfi 1997). The lower panel of Fig. 2 shows the degree of condensation (the fraction of available carbon which is condensed into dust particles) for model P7C14U4 versus the temperature. Depending on the pulsational phase, dust formation starts around 1600 to 1800 K.

3.2. Effect of dust formation

The dynamical models include the formation of dust in the form of amorphous carbon grains. This is expected to be the most abundant type of condensate, as inferred from chemical and thermodynamical considerations (abundances, grain growth time scales) and the almost complete absence of dust features in observed spectra (with the exception of the SiC-feature). The dynamical computation provides the degree of condensation, i.e. the fraction of available carbon (all carbon not blocked in CO due to the molecule's high bonding energy) that is actually condensed into dust particles. This depletion of carbon in the gas phase is taken into account when calculating the molecular partial pressures for the spectrum computation. The fraction of carbon bound in solid particles is subtracted from the element's abundance before solving the detailed chemical equilibrium of the gas phase.

Table 3. Temperature ranges and stellar radii where CO, C_2, CN, HCN, C_3 and C_2H_2 features approximately form according to our models.

molecule	temperature range [K]	radius range [$R_\star$]
CO	$\sim 4200 - \sim 2300$	$\sim 0.6 - \sim 1.3$
C_2	$\sim 4000 - \sim 2100$	$\sim 0.6 - \sim 1.5$
CN	$\sim 4000 - \sim 2500$	$\sim 0.6 - \sim 1.2$
HCN	$\sim 3000 - \sim 1800$	$\sim 0.7 - \sim 1.7$
C_3	$\sim 2500 - \sim 1900$	$\sim 0.8 - \sim 1.6$
C_2H_2	$\sim 2100 - \sim 1300$	$\sim 1.0 - \sim 3.1$

Effects of dust formation on the synthetic spectra get stronger as the degree of condensation of dust in a model becomes larger. In our present models, having low degrees of condensation, the only features which are really affected are those where C_2H_2 contributes. As discussed in Sect. 3.1, C_2H_2 is the only molecule which is formed in large amounts below temperatures of 2000 K. Dust formation starts about temperatures of 1800 K. Therefore, mainly C_2H_2 (being the dominant molecule in these outer regions) is affected by the carbon depletion caused by dust formation.

Fig. 4 shows a maximum light (upper) and a minimum light (lower) spectrum of model P7C14U4, calculated with (full line) and without (dashed line) the depletion of carbon by dust formation taken into account when computing the molecular equilibrium for the spectral synthesis. The 2.5, 3, 3.8 μm features and the 6 to 8 μm region are mostly affected, which are exactly those where C_2H_2 contributes significantly (for a feature identification see Table 2 and Fig. 1).

3.3. Variation of the features

The spectral differences between different phases of a hydrodynamic model mainly arise from the local shock fronts and their propagation through the atmosphere, not from global changes of the structure as in hydrostatic model atmospheres with different stellar parameters. We investigated sequences of 30 to 35 phases of each model. A common feature of all models is that the variation of the molecular features throughout a cycle is less pronounced at wavelengths shortwards of 2 μm than longwards. The main contributing molecules in the 0.5 to 2 μm region are CN and C_2. As one can see from Fig. 2, these molecules are formed deep in the atmosphere where dynamic effects like shocks or a levitation of the atmosphere are less pronounced, therefore the variation of features originating from these regions is small. At wavelengths longwards of 2 μm, molecules like C_2H_2, HCN and C_3 are dominating. They are formed in

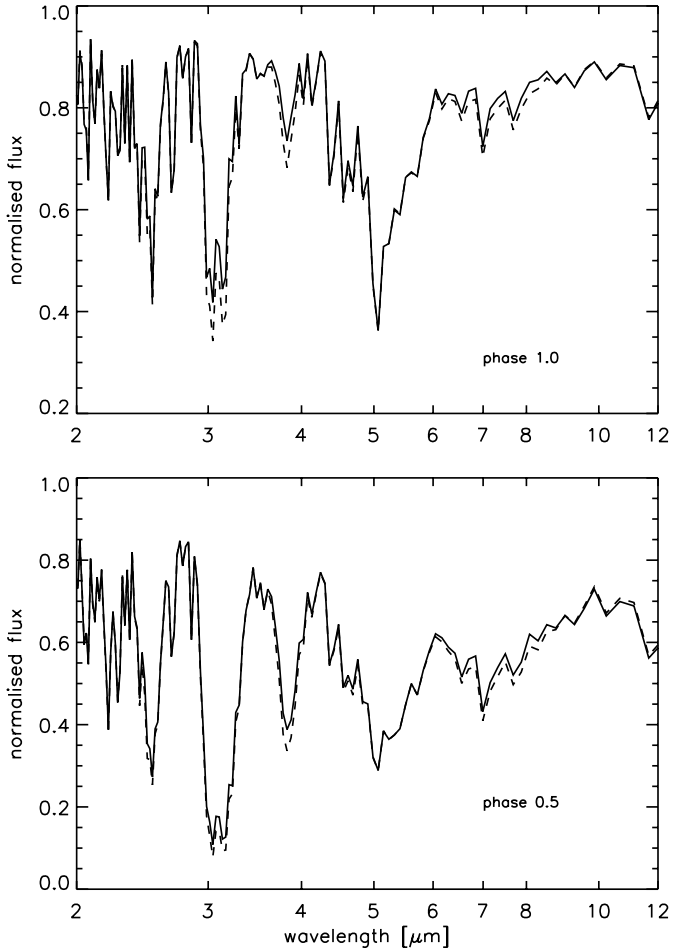

Fig. 4. Synthetic spectra for model P7C14U4 for phase 1.0 (maximum light, *upper*) and phase 0.5 (minimum light, *lower*) with (full) and without (dashed) the depletion of carbon in the gas phase by grain formation taken into account.

regions of the atmosphere where dynamic processes play an important role for the temperature - gas pressure structure and therefore they show sometimes huge variations. The main features in our spectra are summarized in Table 2. Fig. 5 shows synthetic 1 to 12 μm spectra of model P7C14U4 for four phases (full: 1.00, dash-dot: 0.25, dashed: 0.39, dotted: 0.50). The spectrum at phase 0.39 looks already very similar to the one at minimum light. Only the C_2H_2 features become stronger towards phase 0.50. This can be mainly seen at the 3.8 μm feature, but also at 2.5, 3 and $7-9$ μm where C_2H_2 contributes, but due to the blending with other molecules the effect is less pronounced. Calculations for single molecules showed that the variations of the C_2H_2 features follow exactly the bolometric light curve: they are strongest at minimum light (phase 0.5) and weakest at maximum light (phase 1.0). In contrast, the CO, C_2 and CN features are strongest at phase 0.4 and weakest at phase 0.9, respectively. This is also the case for the HCN and C_3 features, but they remain almost constant between phases 0.4 and 0.5 as well as 0.9 and 1.0. In general, features formed at the hottest temperatures peak first, the ones

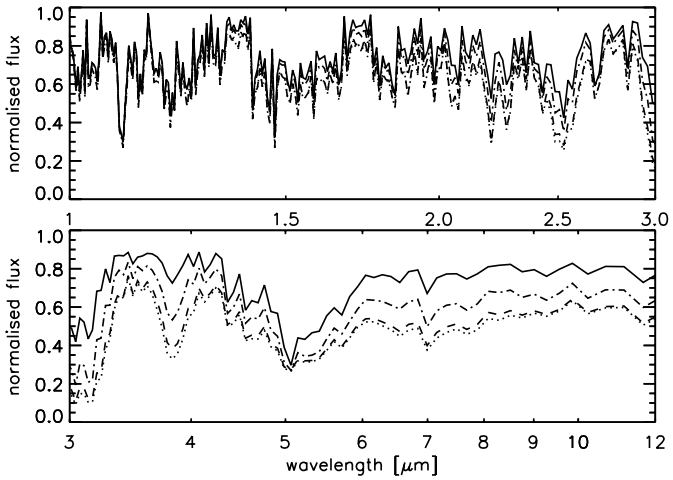

Fig. 5. Synthetic spectra for model P7C14U4 for four phases (full: 1.00, dash-dot: 0.25, dashed: 0.39, dotted: 0.50) between 1 and 12 μm. Note that those features where C_2H_2 contributes (2.5, 3, 3.8 and $7-9$ μm) are strongest exactly at phase 0.5 (minimum light) while all others are already strongest at phase 0.39.

formed at cool temperatures peak last. But in the observed and the synthetic spectra calculated including all molecules (as in Fig. 5), all features with the exception of the uncontaminated 3.8 μm C_2H_2 feature are blends and therefore the effects superimpose, i.e. the intensity of the features remains almost constant over a range of phases around maximum and minimum light.

3.4. Influences of different model parameters on synthetic spectra

We have varied the physical parameters of the models systematically to demonstrate their influence on the synthetic spectra. The influence of the physical parameters on the atmospheric structure for these models is discussed in detail in HJLA98.

Temperature effects

We compare models P7C14U4 with P7TC14U4 and P10C14U4 with P10TC14U4 (model parameters see Table 1). All parameters except the temperature are equal in both cases. A higher temperature gives slightly weaker features and stronger variations in the synthetic spectra as well as a higher level of the pseudo continuum. For an illustration see Fig. 6a. At minimum light the spectra look very similar, the 5.1 μm feature seems to be already saturated while at maximum light especially the 3, 3.8 and the $5-10$ μm region look quite different. A comparison of models P10C14U4 and P10TC14U4 (not plotted here) shows that the spectra look very similar at both phases. In model P10C14U4 the 3 μm feature is already saturated.

Luminosity effects

When comparing models P7C14U4 and P10TC14U4 one sees that a higher luminosity results in stronger features, smaller

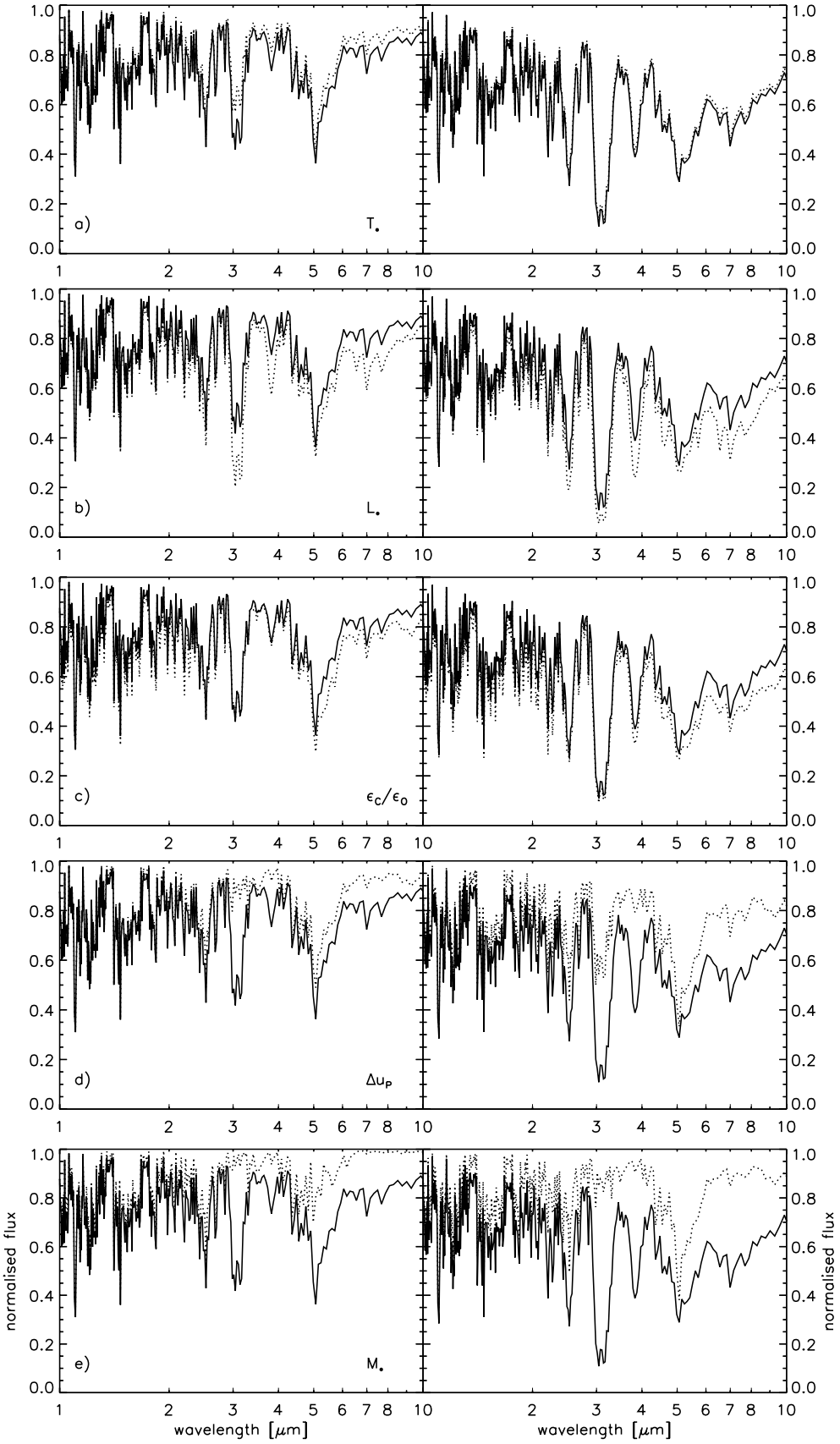

Fig. 6a–e. Normalised synthetic spectra for maximum (*left panel*) and minimum light (*right panel*) showing the influence of different parameters (the full line always shows model P7C14U4): **a** temperature (dotted: P7TC14U4), **b** luminosity (dotted: P10TC14U4), **c** C/O ratio (dotted: P7C18U4), **d** piston velocity (dotted: P7C14U2) and **e** mass (dotted: P7MC14U4).

variations and a deeper level of the pseudo continuum (Fig. 6b). Here, the spectra differ significantly at both phases.

Carbon-to-oxygen effects

A higher $\varepsilon_C/\varepsilon_O$ (P7C14U4/P7C18U4) induces stronger features, slightly stronger variations and a lower level of the pseudo continuum (Fig. 6c). This figure indicates that the higher amount of carbon is used for the formation of C_2 and C_3. When looking carefully one recognizes that the C_2, CO and C_3 features as well as the $7-10\,\mu$m region shows much stronger features at both phases in P7C18U4. In contrast to that the 3 and the $3.8\,\mu$m features look similar in both models at maximum light and differ only slightly at minimum light.

Piston velocity effects

Comparing models P7C14U2/P7C14U4 and P10C18U2/P10C18U4, respectively, yields the following results: a higher piston velocity induces stronger features and variations, and a deeper level of the pseudo continuum (Fig. 6d). At maximum light the spectra look similar up to $2\,\mu$m, while the $2.5\,\mu$m feature is already affected. The $3\,\mu$m feature is very weak and the 3.8 almost not present in P7C14U2. At minimum light the whole spectrum looks different. The lower piston velocity primarily affects those features which are formed in the outer layers of the atmosphere (C_2H_2, HCN). A comparison of P10C18U2 and P10C18U4 (not plotted here) gives the same result, except the 5.1 and $3\,\mu$m features are already saturated in P10C18U4.

Mass effects

A higher mass (P7MC14U2/P7C14U2 and P7MC14U4/P7C14U4) leads to weaker features, smaller variations and a higher level of the pseudo continuum (Fig. 6e). P7MC14U4 and P7MC14U2 show no C_2H_2 and HCN features at all. The atmospheres of these models are not extended enough (pressure at a given temperature is too low) to form them.

Discussion

An interesting point is the behaviour of the 2.5 and $3\,\mu$m features and their ratio in our model spectra at different phases of the light curve. In all our models the $2.5\,\mu$m feature is weaker than the one at $3\,\mu$m at minimum light except in P5C14U2 and P7MC14U2 which are special cases and will be discussed later. At maximum light the situation is different. P7TC14U4 and P7MC14U4 are the only models where the $2.5\,\mu$m feature is stronger than the $3\,\mu$m feature at maximum light. In all other models with a luminosity of 7000 $L_\odot$ both show equal strength at this phase. In contrast, all models with 10000 $L_\odot$ have a weaker 2.5 than $3\,\mu$m feature at maximum light. Therefore the ratio of these two features depends mainly on the luminosity of the model. Only models P5C14U2 and P7MC14U2, which do not show a 3 and $3.8\,\mu$m feature at all phases, behave differently. The densities

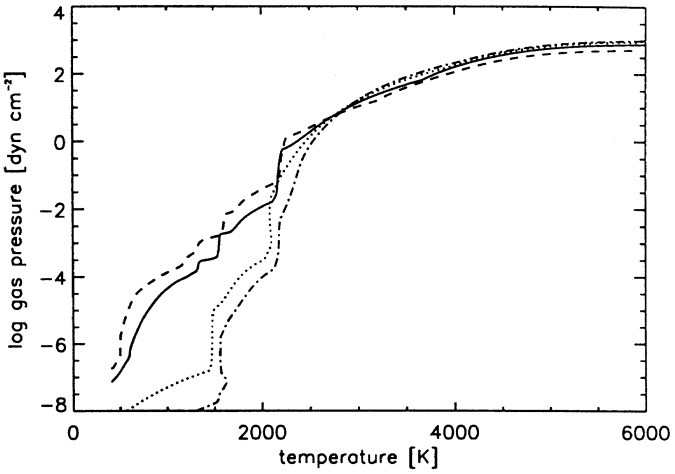

Fig. 7. Gas pressure versus temperature at maximum light for models P7C14U4 (full), P5C14U2 (dash-dot), P7MC14U4 (dotted) and P13C12U4 (dashed). The dashed and the dotted graphs "define" limits in the outer layers ($T < 2000$ K) for yielding reasonable near infrared spectra of AGB carbon stars with optical thin shells as presented in this paper.

of these models are too low in the outer layers, so no C_2H_2 and HCN is formed. Another important point is that some of the features (3 and $5.1\,\mu$m) become saturated around minimum light for models with high luminosities, high carbon-to-oxygen ratios or high piston velocities.

Limiting cases

In this section we want to discuss briefly models P5C14U2, P7MC14U2, P7MC14U4, P13C12U4 and P13C14U4 (for model parameters see Table 1). Model P5C14U2 shows no variation at all, no 3, 3.8 and $7-9$ and only a weak $5.1\,\mu$m feature. This means that the atmosphere of this model is not extended enough (pressure at a given temperature is too low) to form features of polyatomic molecules. Similar is the case for P7MC14U2, but this model shows a small variation at wavelengths greater than $4\,\mu$m. The features are strongest around phase 0.25 and weakest around phase 0.75. Model P7MC14U4 has weak 3 and $3.8\,\mu$m features which vary during a cycle. But still the $3\,\mu$m feature is much weaker than the one at $2.5\,\mu$m. No optical AGB carbon stars without a $3\,\mu$m feature are observed. Thus, these models are not appropriate to describe AGB carbon stars with optical thin shells. In contrast, models P13C12U4 and P13C14U4 result in far too strong and saturated spectral features, so they represent a limit too. But these models have already a higher degree of condensation and therefore the features could become considerably weaker if the dust opacities are taken into account and not only the depletion of carbon as it is done presently. Fig. 7 shows the $T-P_g$ structures of the maximum phase of models P5C14U2 (dash-dot line, not extended enough), P7MC14U4 (dotted line, transition case - 3 and $3.8\,\mu$m features appear at some phases), P7C14U4 (full line, "standard" model) and P13C14U4 (dashed line, too extended in the outer layers). For the method of calculating synthetic spectra

which is presented in this paper, these structures approximately "define" a range yielding reasonable spectra for AGB carbon stars with optically thin shells and thus the range of parameters for our dynamical models.

Comparing the $T-P_g$ structures of two models gives already good hints on how the resulting synthetic spectra compared to each other will differ: if the gas pressure at a fixed temperature is smaller in one model, then the features formed in this temperature range are weaker and if the gas pressure is higher, then the features are stronger.

4. Conclusions

We have presented a systematic analysis of synthetic spectra for carbon stars which result from dynamic model atmospheres. The mean gas opacities used in the dynamic computations (which have a considerable influence on the corresponding spectra) are based on the same molecular data as the frequency-dependent opacities in the spectrum calculation. Although the present models and synthetic spectra are still not completely self-consistent (grey versus OS radiative treatment, spherical versus plane parallel geometry) we stress the progress in modelling NIR-spectra of C-rich AGB stars which are not completely enshrouded by a circumstellar dust shell. A preliminary comparison of our spectra with observations shows good qualitative agreement.

We have investigated the variations of the features in the synthetic spectra calculated from various dynamic atmospheres and have studied how different model input parameters influence the spectra and their variability. Our major results and conclusions are:

- At wavelengths smaller than $2\,\mu$m CN and C_2 are the main contributing molecules, their features do not show large variations. This fact can be understood when keeping in mind that these features are formed in deep atmospheric layers (T higher than 3500 K) where dynamic effects such as shocks and levitation are smaller. In the wavelength region longwards of $2\,\mu$m CO, C_3, HCN and C_2H_2 dominate our spectra, and the three latter ones are formed at low temperatures, i.e. in regions where dynamic effects play an important role. Therefore it is not surprising that these features show large variations with phase.
- Especially the piston velocity of a model is responsible for the amount of variation in the resulting spectrum, while parameters like the carbon-to-oxygen ratio, luminosity, temperature or mass mainly influence the average feature strength.
- Spectral features longwards of $2\,\mu$m are strongest at minimum light (phase 0.50) and weakest at maximum light (phase 1.00).
- When calculating synthetic spectra for a model where one parameter was changed in comparison to a fixed standard model (P7C14U4), the spectra result in:
  - higher luminosity: stronger features
  - higher mass: weaker features
  - higher effective temperature: weaker features
  - higher $\varepsilon_C/\varepsilon_O$: stronger features
  - higher piston velocity: stronger features

We have based our present analysis of the overall shape and variation of the synthetic spectra on relatively low resolution opacity sampling absorption coefficients, which has allowed us to analyse a large parameter space of basic stellar input. Recent ISO observations of cool carbon stars (Yamamura et al. 1998, Hron et al. 1998, Aoki et al. 1998) at higher resolution than the synthetic spectra we present here, have demonstrated the need for more detailed opacity data for quantitative analysis of the high quality ISO spectra.

At present, f-values available in different studies in the literature of some of the diatomic bands (mainly from C_2) differ from one another by approximately a factor of 10, and the values of the band strengths of several of the bands due to C_2H_2 and to C_3 are uncertain within a factor of 10 too, although the statistical accuracy, which is important for the structural computations, is considerably better than this. In future studies at higher resolution we hope to be able to improve the estimates of the individual band intensities.

Other major improvements which we intend to add to future studies include frequency dependent opacities in the model computations, a self-consistent treatment of the basic pulsational physics, the inclusion of dust opacities and of sphericity in the spectral synthesis, and taking the effects of velocity fields on opacities and radiative transfer into account. Some of these points face so large theoretical and/or computational challenges that their immediate solution must not be expected. We have, however, been able to perform preliminary tests on the effects of spherical radiative transfer, which indicate that the molecular features on average become weaker compared to the results presented here, but that the relative tendencies of how the model parameters influence the spectra remain the same as in the present study.

Acknowledgements. This work is supported by the Austrian Science Fund (FWF, project numbers S7308-AST, J01283-AST and J1487-PHY) and by the Danish Natural Science Research Council. We thank J. Hron (IfA Vienna) for inspiring discussions, A. Gautschy (Basel) for providing us with the program solving the stellar structure equations, as well as T. Tsuji (Tokyo) and B. Plez (Lund) for communications concerning C_3. RL acknowledges a "Doktorandenstipendium" of the Austrian Academy of Sciences.

References

Alvarez R., Plez B., 1998, A&A 330, 1109
Aoki W., Tsuji T., Ohnaka K., 1998, A&A 340, 222
Aringer B., Höfner S., Wiedemann G., et al., 1999, A&A, in press
Beach T.E., Willson L.A., Bowen G.H., 1988, ApJ 329, 241
Bessell M.S., Brett J.M., Scholz M., Wood P.R., 1989, A&A 213, 209
Bessell M.S., Scholz M., Wood P.R., 1996, A&A 307, 481
Bowen G.H., 1988, ApJ 329, 299
Bowen G.H., Willson L.A., 1991, ApJ 375, L53
Ekberg U., Eriksson K., Gustafsson B., 1986, A&A 167, 304
Feast M.W., Glass I.S., Whitelock P.A., Catchpole R.M., 1989, MNRAS 241, 375

Fleischer A.J., Gauger A., Sedlmayr E., 1992, A&A 266, 321
Gail H.P., Sedlmayr E., 1988, A&A 206, 153
Gauger A., Gail H.P., Sedlmayr E., 1990, A&A 235, 345
Goebel J.H., Bregman J.D., Goorvitch D., et al., 1980, ApJ 235, 104
Goorvitch D., Chackerian C. Jr., 1994, ApJS 91, 483
Gustafsson B., Bell R.A., Eriksson K., Nordlund Å., 1975, A&A 42, 407
Helling C., Jørgensen U.G., Plez B., Johnson H.R., 1996, A&A 315, 194
Höfner S., Dorfi E.A., 1997, A&A 319, 648
Höfner S., Jørgensen U.G., Loidl R., 1998a, Proc. ISO's View on Stellar Evolution, Ap&SS 255, 281
Höfner S., Jørgensen U.G., Loidl R., Aringer B., 1998b, A&A 340, 497 (HJLA98)
Hron J., Loidl R., Höfner S., et al., 1998, A&A 335, L69
Iben I., 1984, ApJ 277, 333
Irwin A.W., 1981, ApJS 45, 621
Jørgensen U.G., 1989a, ApJ 344, 901
Jørgensen U.G., 1997, in: van Dishoek E.F. (ed.) Molecules in Astrophysics: Probes and Processes. Proc. IAU Symp. 178, Kluwer, p. 441
Jørgensen U.G., Almlöf J., Gustafsson B., Larsson M., Siegbahn P.E.M., 1985, J. Chem. Phys. 83, 3034
Jørgensen U.G., Larsson M., 1990, A&A 238, 424
Jørgensen U.G., Almlöf J., Siegbahn P.E.M., 1989b, ApJ 343, 554
Jørgensen U.G., Johnson H.R., Nordlund Å., 1992, A&A 261, 263
Lambert D.L., Gustafsson B., Eriksson K., Hinkle K.H., 1986, ApJS 62, 373
Loidl R., Hron J., Höfner S., et al., 1997, Ap&SS 251, 243
Querci F., Querci M., Tsuji T., 1974, A&A 31, 265
Tsuji T., 1973, A&A 23, 411
Tsuji T., Ohnaka K., Aoki W., 1997, In: Okuda H., Matsumoto T., Roellig T. (eds.) Proc. of DiffuseInfraredRadiationandtheIRTS. A.S.P. Conf. Series Vol. 124
Windsteig W., Dorfi E.A., Höfner S., Hron J., Kerschbaum F., 1997, A&A 324, 617
Winters J.M., Fleischer A.J., Le Bertre T., Sedlmayr E., 1997, A&A 326, 305
Yamamura I., de Jong T., Justtanont K., Cami J., Waters L.B.F.M., 1998, In: Proc. ISO's View on Stellar Evolution, Ap&SS, in press